IEEE Access
Multidisciplinary : Rapid Review : Open Access Journal

Received July 29, 2020, accepted August 11, 2020, date of publication August 14, 2020, date of current version August 25, 2020.
Digital Object Identifier 10.1109/ACCESS.2020.3016686

Reliability Analysis and Design of MMC Based on Mission Profile for the Components Degradation

GAOTAI LV, (Graduate Student Member, IEEE), WANJUN LEI, (Member, IEEE), MENG WANG, CHUNLIN LV, (Graduate Student Member, IEEE), AND JIAQI ZHAO
School of Electrical Engineering, Xi'an Jiaotong University, Xi'an 710049, China
Corresponding author: Wanjun Lei (leiwanjun@mail.xjtu.edu.cn)

This work was supported by the National Key Research and Development Plan under Grant 2018YFB0905800.

ABSTRACT In the field of high voltage level applications, modular multi-level converter (MMC) has the definite advantages of low power loss and modularity and there have been many studies on its reliability. Some researches focus on the degradation of physical characteristics in the lifetime prediction of key devices, but the degradation of physical characteristics has not been directly used in the research of MMC system level reliability. The traditional exponential distribution failure rate is constant while the Monte Carlo method assumes the random distribution of multiple devices. Neither of these two methods can describe the reliability of a single device with physical characteristics degradation. This article presents a system level MMC reliability analysis and design method based on MMC mission profile and insulated-gate bipolar transistor (IGBT) lifetime degradation. According to the IGBT current and power loss in MMC, the annual mission profile and junction temperature result are analyzed by rainflow counting algorithm. In terms of device degradation, the thermal network updating method is used to calculate the life of IGBT in different time, and the reliability analysis method based on exponential distribution is improved. To optimize the redundancy design of the system, the multi-objective function optimization is processed.

INDEX TERMS Modular multi-level converter, lifetime prediction, device degradation, failure rate, reliability analysis, redundancy optimization.

I. INTRODUCTION

Modular multi-level converter (MMC) [1] which is widely used in high voltage direct current (HVDC) field has obvious advantages in hydropower generation. For example, the MMC Fengning station of Zhangbei HVDC project is mainly used for power supply, water storage, and hydropower transmission of Fengning hydropower station. In order to deliver power generated by hydropower far away, the voltage level must be improved and utilization of MMC is considerable. The cost of MMC is expensive and its modularity is easy to maintain, which makes people have a higher demand for its reliability.

The aspect of MMC reliability research can be divided into component level and system level. In recent years, some researches [2]–[4] on the lifetime prediction of key devices have used the rainflow algorithm to analyze the long-time scale mission profile fluctuation data. The fatigue damage and lifetime prediction are carried out by substituting the analysis results into Coffin-Manson [5], Norris-Landzberg [6], Bayerer [7], and other models. From the aspect of physical failure mechanism, the main causes of failure are solder layer fatigue deterioration [8] and bonding lead wire falling off of IGBT. Among them, with the accumulation of load, the thermal resistance of solder layer increases gradually, which is generally considered as failure when it increases by 20%.

Due to the failure rate of traditional exponential distribution is constant, the reliability analysis cannot be accurate in actual working condition. From device level lifetime prediction to system level reliability, a Monte Carlo method is proposed to analyze system level reliability [9] based on the working condition profile. Random distribution is used to combine device lifetime prediction based on failure mechanism with system level unreliability. In the system level reliability analysis, there are three main methods to establish the reliability structure, reliability block diagram (RBD) [10], fault tree analysis (FTA) [11] and Markov analysis (MA) [12].

The associate editor coordinating the review of this manuscript and approving it for publication was Feifei Bu.

This work is licensed under a Creative Commons Attribution 4.0 License. For more information, see https://creativecommons.org/licenses/by/4.0/

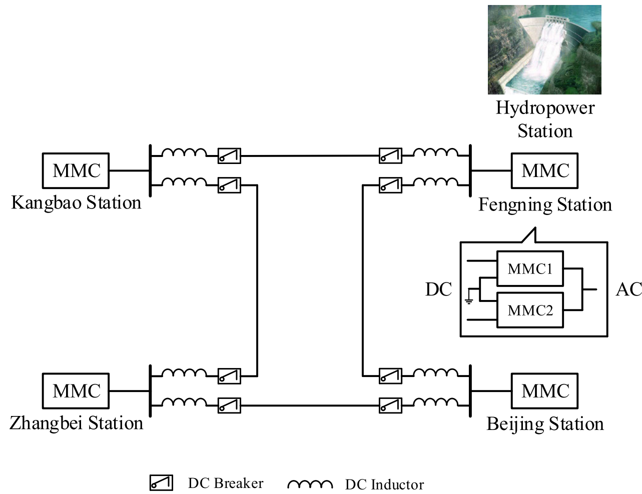

FIGURE 1. Zhangbei HVDC transmission project.

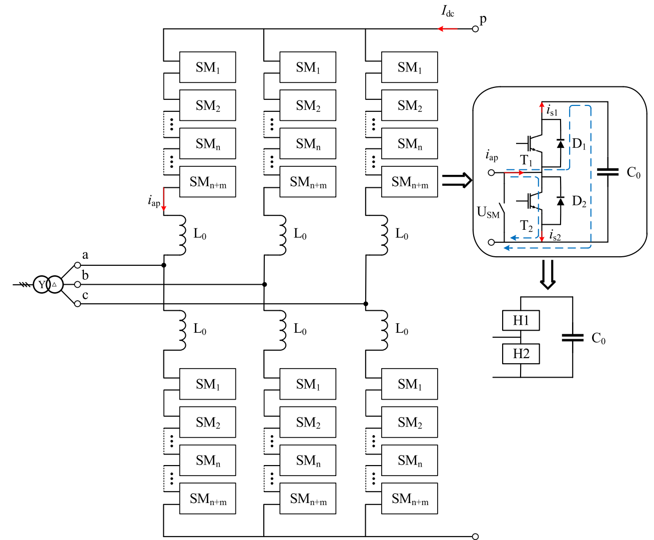

FIGURE 2. Half-bridge MMC topology.

A reliability analysis method based on different redundant backup modes is proposed [13], in which the k/n(G) [10] model is more widely used in the case of active redundancy. With consideration of economic factors, the failure manual based failure rate calculation is implemented at the device level, while RBD and k/n(G) are utilized to evaluate the reliability at the system level [14].

However, there are few studies on the degradation of device level performance, such as the influence of IGBT solder layer thermal resistance on system level reliability and device level failure efficiency. According to the annual mission profile and power mission profile, this article starts at the aspect of key device degradation, evaluates IGBT and capacitor damage with working conditions. Then, the change of lifetime and failure rate with time have been calculated in this condition. To improve the reliability evaluation method under the traditional exponential distribution, a failure rate conversion method based on the actual working condition mission profile and aging analysis is proposed in this article. The difference from Monte Carlo method is that it analyzes the time-varying loss efficiency of a single device, while Monte Carlo method assumes that multiple device parameters are normally distributed. After comparing the reliability analysis results with Monte Carlo method, multi-objective function optimization is executed to design redundancy based on reliability, and the optimal number of redundancy modules in economy as well as reliability is given correspondingly.

II. MMC MISSION PROFILE ANALYSIS

In the reliability analysis, in order to analyze the reliability of components and systems in the actual operation condition, researchers usually consider mission profile as input data and process the data to get the lifetime prediction results.

For instance, in Fig. 1, Zhangbei project, MMC is used as a voltage sourced converter (VSC) in HVDC transmission project. Fig. 2 is a half-bridge MMC topology of one pole from bipolar MMC in Fengning station of Zhangbei project as well as its parameters can be seen from Table 1.

TABLE 1. MMC specifications of Fengning station.

Parameter	Parameter
System rated active power P	750MW
Rated DC-link voltage U_{dc}	500kV
DC side current Idc	1.5kA
Number of submodules N	232
Submodule capacitor C_0	7mF
Arm inductor L_0	75mH
Fundamental frequency f	50Hz
Submodule switching frequency f_s	150Hz

A. POWER LOSS ANALYSIS AND EVALUATION

To process the stress data and gain the corresponding IGBT junction temperature, an analysis of the IGBT power loss in submodules from MMC is essential.

When MMC operates in three-phase symmetry, the DC current is evenly distributed in the three-phase bridge arm, and the AC current is evenly distributed in the upper and lower bridge arms of each phase. Taking phase a as an example, the current of the upper and lower bridge arms can be expressed as

$$i_{ap} = \frac{1}{3}I_{dc} + \frac{1}{2}I_{\mathrm{m}} \sin(\omega t + \varphi) \quad (1)$$

$$i_{an} = \frac{1}{3}I_{dc} - \frac{1}{2}I_{\mathrm{m}} \sin(\omega t + \varphi) \quad (2)$$

I_m is the peak value of phase a current, while ω is the fundamental angular frequency and ϕ represents the AC power factor angle of MMC. The voltage of the upper and lower bridge arms of phase a can be expressed as

$$u_{ap} = d_{a,upper} U_{dc} \quad (3)$$

$$u_{an} = d_{a,lower} U_{dc} \quad (4)$$

where a,b,c means different phases, *upper,lower* represents upper and lower bridge arms, d is the duty ratio. MMC should ensure that the DC side voltage value is U_{dc}, and the input duty ratio of the upper and lower bridge arms of phase a can

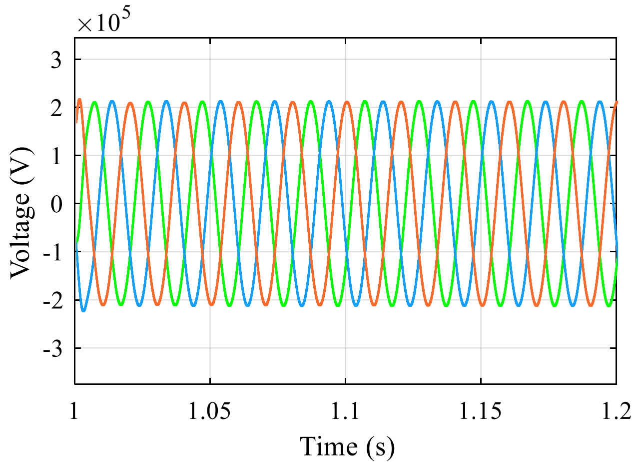

FIGURE 3. AC side voltage in Fengning station simulation.

be calculated

$$n_{a,up}U_{dc} + n_{a,down}U_{dc} = U_{dc} \tag{5}$$
$$n_{a,down}U_{dc} - \frac{U_{dc}}{2} = U_m \sin \omega t \tag{6}$$
$$n_{a,up} = \frac{1}{2}(1 - k \sin \omega t) \tag{7}$$
$$n_{a,down} = \frac{1}{2}(1 + k \sin \omega t) \tag{8}$$

U_m is the peak value of phase a voltage showed in Fig. 3, and the modulation ratio is $k = 2U_m/U_{dc}$.

Suppose the MMC system impedance is in ideal condition [3] we can get

$$I_{dc} = \frac{3}{4}kI_m \cos \varphi \tag{9}$$

When the submodule is put into operation, the bridge arm current flows through H_1 to charge and discharge the submodule capacitor; when the submodule is cut out, the bridge arm current flows through H_2. The equivalent current flowing through submodules H_1 and H_2 in a power frequency cycle can be calculated, taking the submodule of a-phase upper bridge arm as an example

$$i_{H1} = n_{a,up}i_{ap} \tag{10}$$
$$i_{H2} = n_{a,down}i_{ap} \tag{11}$$

To estimate the thermal stress of the switch device, the current stress in T_1 and T_2, D_1 and D_2 must be calculated separately. According to Fig. 4, when the bridge arm current flows in the positive direction, i.e. in ($\alpha 1$, $\alpha 2$), it flows through D_1 or T_2; when the bridge arm current flows in the reverse direction, i.e. in ($\alpha 2$, $\alpha 3$), it flows through T_1 or D_2. The average and effective value of the current flowing through IGBT and diode in a power frequency cycle can be estimated respectively.

$$i_{T_1 avg} = \frac{1}{2\pi} \int_{\alpha_2}^{\alpha_3} i_{S1} d\omega t \tag{12}$$
$$i^2_{T_1 rms} = \frac{1}{2\pi} \int_{\alpha_2}^{\alpha_3} n_{a,up}i_{ap} d\omega t \tag{13}$$

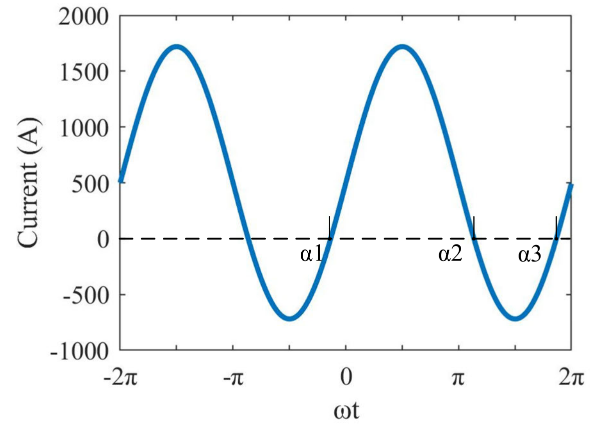

FIGURE 4. AC current of bridge arm on a single phase.

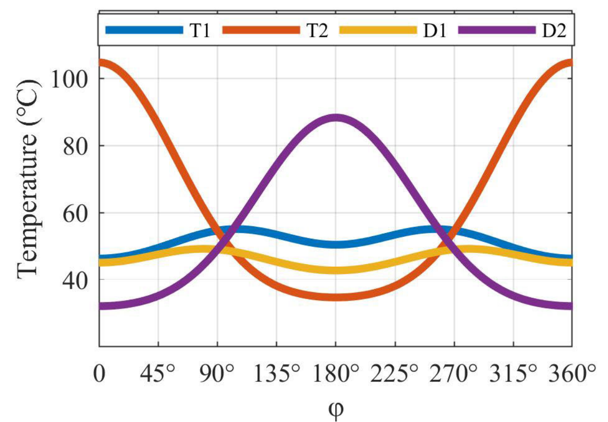

FIGURE 5. Junction temperature variation at different power factor angle. In the reactive power condition, the junction temperature of each device is almost the same.

Taking T_1 as an example, the average current and RMS are obtained. By substituting equations (12), (13) into equations (14) and (15), IGBT loss P_T and diode loss P_D can be calculated, which are the essential variables of junction temperature evaluation showed in equation (16)

$$\begin{aligned} P_T &= P_{con,T} + P_{sw,T} \\ &= V_{T0}i_{Tavg} + R_{CE}i^2_{Trms} + f_s\left(a_T + b_T i_{Tavg} + c_T i^2_{Trms}\right) \end{aligned} \tag{14}$$

$$\begin{aligned} P_D &= P_{con,D} + P_{rec,D} \\ &= V_{D0}i_{Davg} + R_D i^2_{Drms} + f_s\left(a_D + b_D i_{Davg} + c_D i^2_{Drms}\right) \end{aligned} \tag{15}$$

$$T_j = P_{T/D}(\sum_{i=1}^{4} R_i + R_{ch}) + (P_T + P_D)R_{ha} + T_a \tag{16}$$

where $R_{ha} = 0.0356$ K/W is the thermal resistance when using a water-cooled heatsink. Table 2 shows Foster thermal network [15] parameters which are extracted from the datasheet of FZ1500R33HL3 IGBT.

Fig. 5 shows that under active power transmission, the junction temperature of T_2 is higher than that of T_1, and the greater the active power is, the greater the gap between

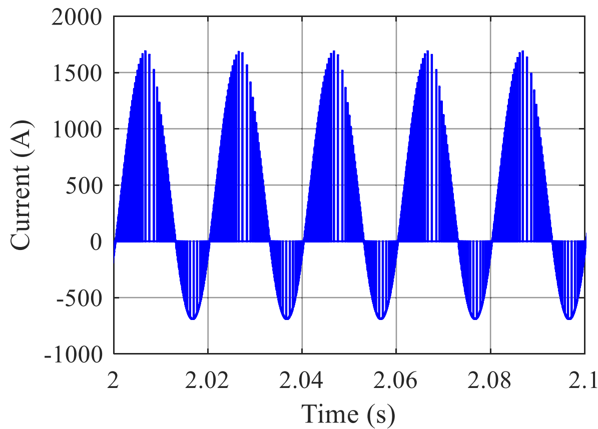

FIGURE 6. Capacitor current.

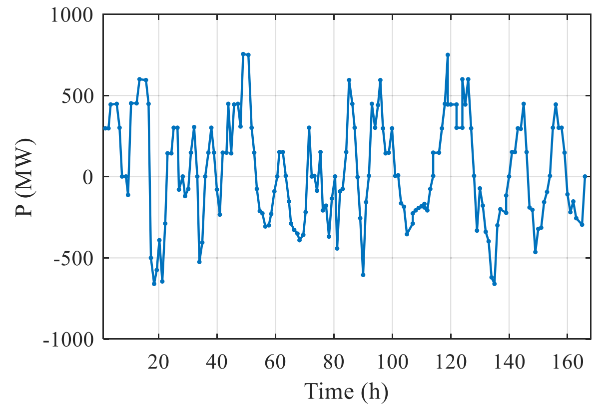

FIGURE 7. One week power mission profile.

TABLE 2. Parameters of the fourth-order foster model.

Device	Parameter	Value			
IGBT	Ri(K/W)	0.001	0.003869	0.00146	0.001002
	τ(s)	0.003	0.042	0.256	4.984
Diode	Ri(K/W)	0.002414	0.006266	0.002787	0.001509
	τ(s)	0.002	0.036	0.252	5.587

junction temperature of T_2 and T_1 is. Moreover, the average junction temperature of D_2 is the highest in the state of maximum active power rectification and T_2 is the highest in the state of the inverter [3], [16]. The junction temperature of T_1 and D_1 is relatively stable in the whole operation range, so the aging of T_2 module will be significantly faster than T_1.

It can be seen that the steady-state capacitor C_0 current of submodule under rated power in Fig. 6. With the calculation of I_{rms}, three AVX metalized polypropylene film (MPPF) capacitors DKTFM2∗#E2577 [17] are used in parallel in consideration of safety and reliability redundancy. Then the hot spot temperature θ_{HS} is calculated according to the formula given in the datasheet.

$$P_{cap} = P_j + P_d = I_{rms}^2 R_s + \frac{I_{rms}^2}{wC}\delta_0 \tag{17}$$

$$\theta_{HS} = T_a + P_{cap} R_{th} \tag{18}$$

where P_{cap} represents the total losses, R_s is equivalent series resistance (ESR) for Joule losses P_j, δ_0 is 3×10^{-4} for dielectric losses P_d, R_{th} is thermal resistance between hot spot and ambient air, and T_a is the ambient temperature.

B. LIFETIME PREDICTION BY STRESS DISTRIBUTION

As the existing IGBT lifetime prediction models Coffin-Manson, Norris-Landzberg and Bayerer contain the average temperature and temperature fluctuation in a cycle, the rainflow algorithm is the usual implementation to deal with the mission profile for this kind of IGBT lifetime prediction, considering the actual operating conditions. The most common modulation methods used in MMC are carrier phase shifted SPWM (CPS-SPWM) [28] and nearest level modulation (NLM) [29]. Among them, the CPS-SPWM strategy determines the trigger pulse sequence of switching devices by comparing the sinusoidal modulation wave with a group of triangular carriers with different phases. This strategy can ensure that the power loss of each submodule of MMC is uniform and has good harmonic characteristics, which is more suitable for the case of less MMC submodules. The nearest level modulation (NLM) is a method that uses step wave to control the submodule switching on or off. The desired modulation voltage is divided by the capacitor voltage of a single submodule, and then the number of submodules is rounded as the final input number, that is, the sum of submodule voltages is used to approximate the modulation wave as much as possible, and the PWM pulse of all submodules is obtained. Under the NLM strategy and traditional submodule capacitor voltage sharing control strategy, the switching action of the device is very uncertain, and the switching frequency is difficult to calculate. It is found that the average switching frequency of the switching devices in the power frequency cycle is about three times of the fundamental frequency (150Hz). The MMC with NLM strategy can approach the modulation wave in a large working range, and the harmonic content of the output voltage is small, so it is suitable for HVDC transmission system with a large number of submodules. Therefore, in Zhangbei project, the MMC with more than 200 modules in a single arm uses NLM strategy.

The one-week power mission profile [18] of Fengning hydropower station is shown in Fig. 7, positive value of power means that the water pumping of the hydropower station needs the DC grid side inverter power supply, and negative value represents that the power generation rectifies to the grid side. With the combination of power and annual temperature mission profile [19] in Fig. 8 (a), the disordered data is cyclized by rainflow algorithm to obtain the stress distribution as shown in Fig. 9. Fig. 8 (b) and (c) are junction temperature stresses at constant full load power. From what has been depicted in Fig. 8, T_2 junction temperature is the highest in constant inverter mode, D_2 is the lowest, and vice versa in rectifier mode. Junction temperature fluctuation

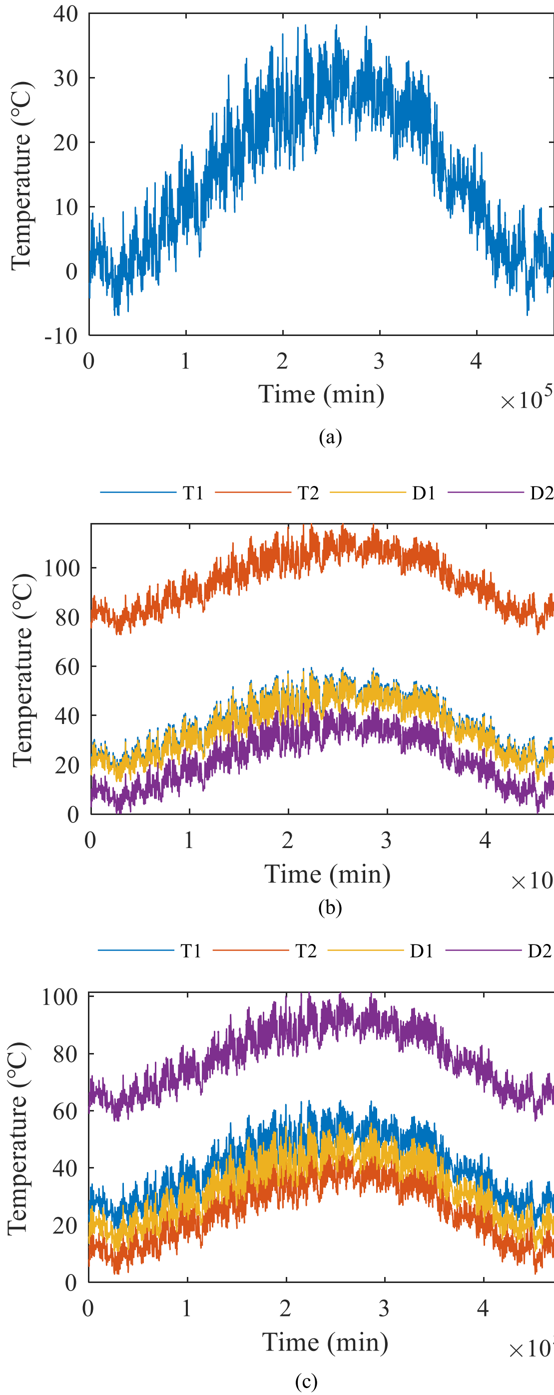

FIGURE 8. Annual mission profile without variable operation. (a) Ambient temperature. (b) Inverter mode. (c) Rectifier mode.

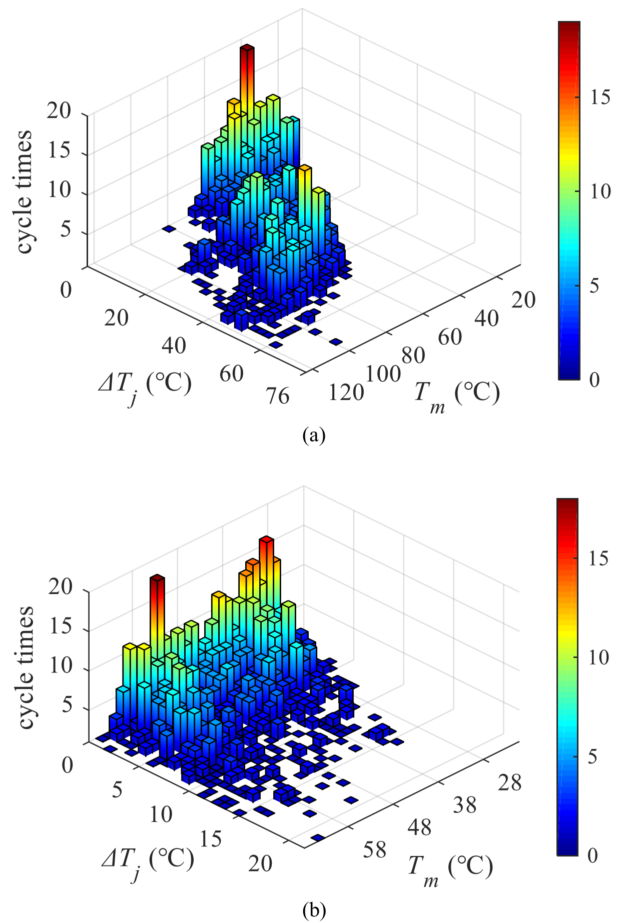

FIGURE 9. Stress distribution after processing annual mission profile by rainflow algorithm. (a) IGBT2. (b) IGBT1.

of T_1 and D_1 change little in both conditions. Compared with T_1, stress distribution of T_2 is more concentrated and has more frequencies of higher ΔT_j. However, T_m with the highest cycle time between two components is close. There are massive data points in minutes that slows the calculation speed of rainflow algorithm, and a small amount of stress in the stress distribution cannot be seen clearly. In this article, the stress distribution Fig. 9 is simplified to profile in hours, and the annual cumulative damage amount is almost the same as before.

The lifetime of IGBT and diode are able to be predicted by substituting the annual stress distribution into the Norris-Landzberg model [4], [6]

$$N_f = Af^{\alpha}(\Delta T_j)^{\beta} e^{\frac{E_a}{k(T_m+273)}} \tag{19}$$

where N_f is the predicted life after each cycle, f is the cycle frequency, k is the Boltzmann constant, E_a is the activation energy, T_m is the maximum junction temperature over a thermal cycle, ΔT_j is the fluctuation of junction temperature.

According to Miner's rule [20], the total damage D and predicted life L under the mission profile are obtained by calculating the damage amount after each cycle, as shown in (20) and (21).

$$D = \sum_{i=1}^{N} \frac{n_i}{N_{f,i}} \tag{20}$$

$$LD = 1 \tag{21}$$

For the MPPF capacitor in the submodule, I_{rms} is the main source of internal heat generation. Therefore, under the constant DC voltage control scheme, the hot spot temperature

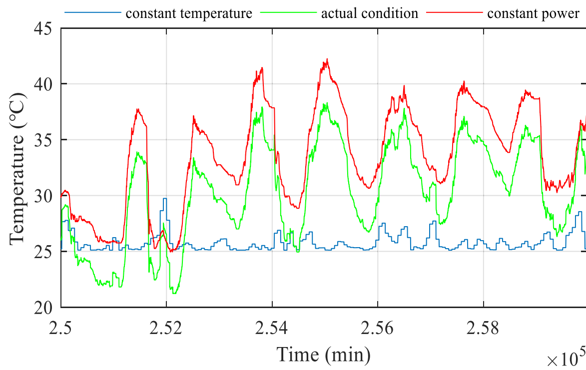

FIGURE 10. Hot spot temperature under different operating conditions. The ambient temperature is 25 °C under constant temperature condition, and MMC operates at rated power under constant power condition.

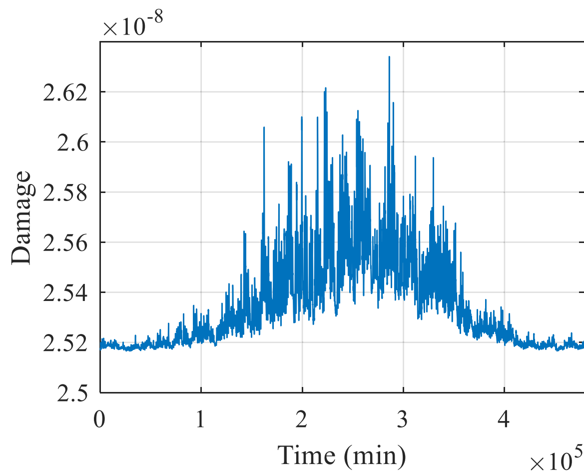

FIGURE 11. C_0 damage distribution per year under actual condition.

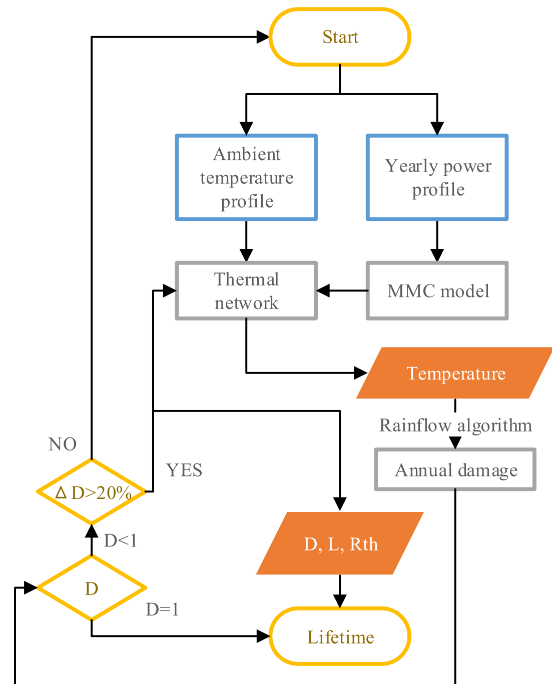

FIGURE 12. Flowchart of segmented extraction from device degradation related data.

TABLE 3. Annual damage with Rth variation.

Device	Damage(year)				
	Rth	1.04Rth	1.08Rth	1.12Rth	1.16Rth
T1	0.000535	0.000543	0.000551	0.000561	0.00057
D1	0.000275	0.000279	0.000285	0.00029	0.000294
T2	0.044401	0.045763	0.047160	0.048587	0.05006
D2	0.010526	0.010969	0.01143	0.011923	0.012388

under different working conditions and ambient temperature as shown in Fig. 10 should be analyzed firstly.

Since the mission profile based on the hot spot temperature in operation condition have been processed, the failure rate calculation formula in datasheet is used as the lifetime original data source, which is equivalent to damage D in the case of severe conditions and reliability exponent distribution. Thus, the damage amount under the mission profile is shown in Fig. 11 and the equivalent annual damage D_{cap} under the linear fatigue cumulative damage can be evaluated.

III. PERFORMANCE DEGRADATION ANALYSIS

The parameters of nonlinear thermal resistance fatigue accumulation model [21] need a large number of experimental data fitting, and the parameter from it is not universal. A thermal network updating method [22] based on solder layer aging is proposed, in which each segment of damage updates the thermal resistance of IGBT once in the fatigue accumulation calculation. In accordance with the analysis of junction temperature and life prediction under the analytical lifetime model, this method can be used to obtain the lifetime of MMC in the temperature and operation condition of considering IGBT aging factors. When the thermal network is not updated with aging, the damage amount of the annual mission profile is the same every year. By using the method shown in Fig. 12, the damage amount that increases gradually with time can be evaluated as shown in Fig. 13. T_2 and D_2 have higher damage per year and higher damage rate with service time than T_1 and D_1. Furthermore, the damage of each component in Table 3 can be calculated.

Considering that the increase of solder layer thermal resistance between different layers has little effect on lifetime prediction [23], it is approximately supposed that IGBT fails when the overall thermal resistance Rth in Foster thermal network rises to 1.2Rth. Through substituting into the actual working condition, we can see that when considering the increase of the thermal resistance of solder layer with the service time, the damage amount of single-cycle also increases with each year as Fig. 14 showed.

Because of the high-reliability MPPF with self-healing characteristics, the aging phenomenon is mainly reflected in the increase of ESR and the decrease of capacitance. Some researchers [24] have been carried out to test the overstress acceleration of aging phenomenon. In terms of the changes of

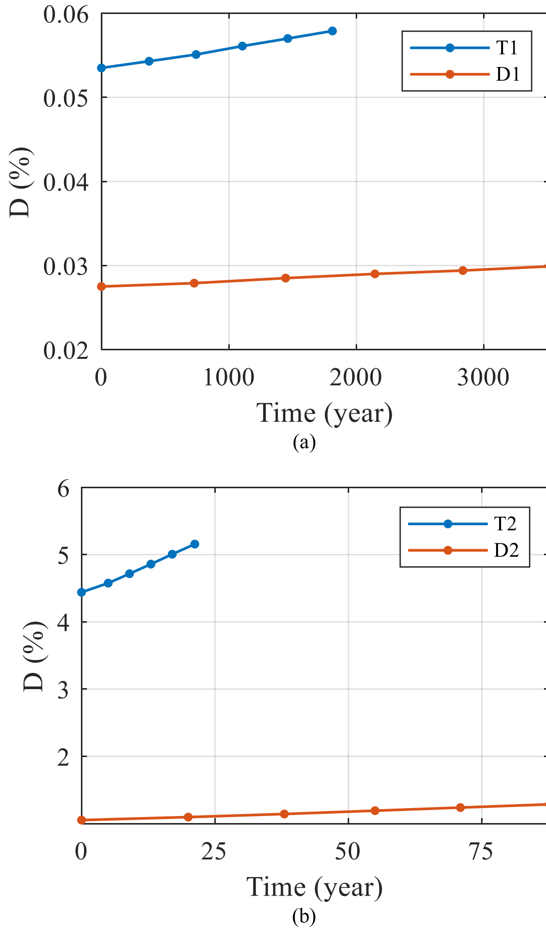

FIGURE 13. IGBT and diode single mission profile damage growth with time.

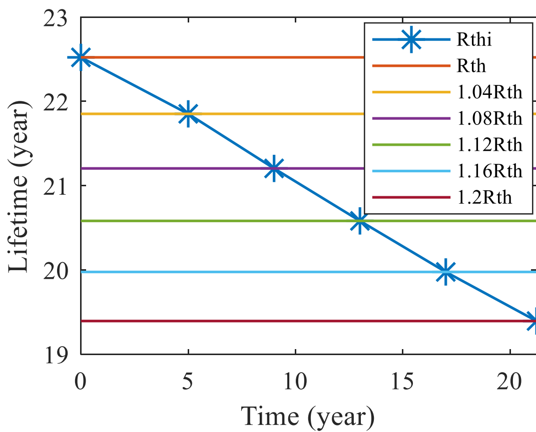

FIGURE 14. Lifetime prediction of single mission profile with increasing thermal resistance over time. The lifetime here refers to the prediction results of undamaged devices in the current thermal resistance state without consideration of damaged amount.

ESR and capacitance, the annual damage with different aging degrees is analyzed. However, the effect of degradation on damage is not obvious in actual working conditions, and the annual damage increase caused by performance degradation can be seen obviously under constant high stress, as shown in Fig. 15 that ESR increment and capacitance reduction are divided into five sections. When $\Delta = 1$, $\Delta ESR = 120\%$, $\Delta C = 5\%$, the deterioration of ESR is more important than that of capacitance in this case.

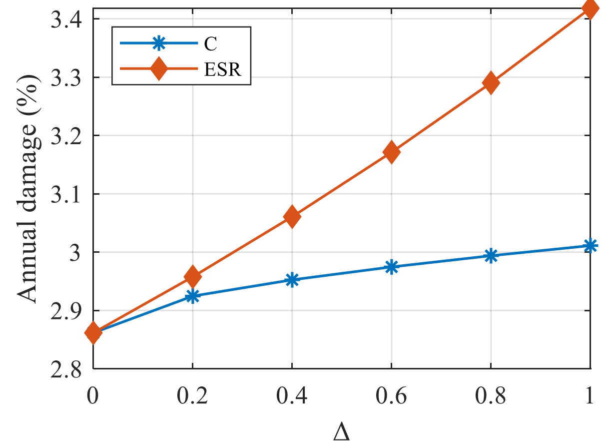

FIGURE 15. Annual damage with capacitance and ESR performance degradation. $T_a = 50°$, $I_{rms} = 400A$.

IV. SYSTEM RELIABILITY ANALYSIS AND DESIGN

To obtain the segmented lifetime prediction of device degradation, it is inevitable to process the mission profile data by using the rainflow algorithm. Then, the relationship between lifetime and degradation is converted to reliability and failure rate, and the system level reliability analysis as well as design are carried out. The MMC reliability analysis and design method based on the physical performance degradation of devices are proposed as shown in Fig. 16.

A. FAILURE RATE CONVERSION

In the calculation of failure rate, the lifetime prediction obtained by the traditional exponential [12] distribution model is constant, which is not suitable for this case. Weibull distribution fitting [9] requires Monte Carlo simulation for each parameter, but it cannot reflect the effect of physical performance parameter degradation on the failure rate of a single device. The corresponding Weibull distribution parameters of submodule devices are shown in Table 4 and the fitting process is depicted in Fig. 17. λ_e is the aging failure rate under working condition and lifetime has been evaluated. For the parameters of lifetime prediction model, the Monte Carlo simulation shows that 10,000 samples obey the normal distribution with deviation of 0.1. (22) and (23) are the realization of Monte Carlo simulation using Weibull distribution fitting results to convert to reliability

$$f(t) = \frac{\beta}{\eta}(\frac{t}{\eta})^{\beta-1}\exp[-(\frac{t}{\eta})^{\beta}] \tag{22}$$

$$R(t) = 1 - F(t) = 1 - \int_0^t f(x)dt = \exp[-(\frac{t}{\eta})^{\beta}] \tag{23}$$

where $f(t)$ is failure probability density function, $F(t)$ is failure cumulative distribution function and $R(t)$ is reliability.

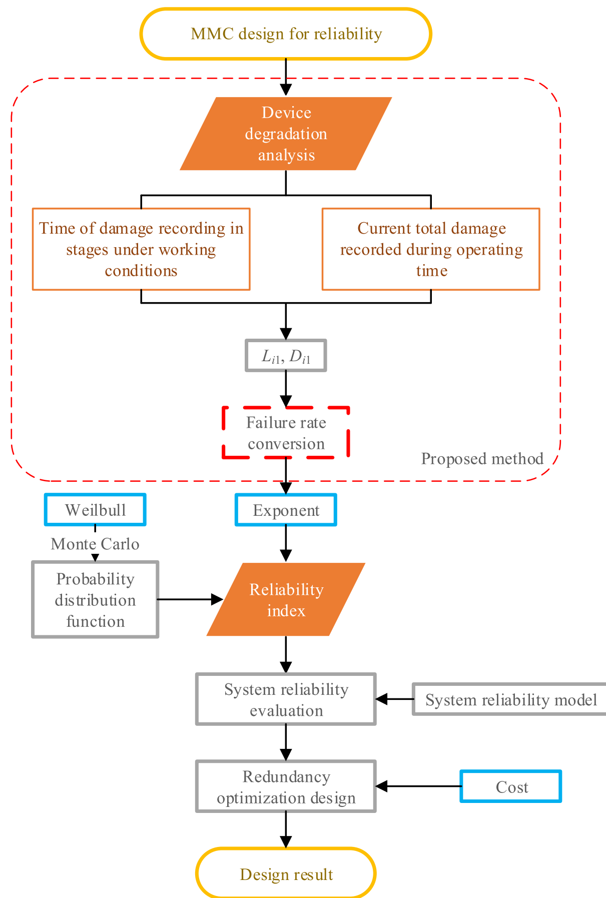

FIGURE 16. MMC reliability design process considering degradation of device performance parameters and actual working conditions.

TABLE 4. Lifetime prediction and failure rate.

Device	Lifetime (year)	Weibull		Failure Rate
		β	η	λ_e
T1	1812.5	1.40939	7727.46	0.000556
D1	3515.83	1.39665	14907.8	0.000284
T2	21.23	1.31052	108.164	0.047103
D2	87.7	1.33723	354.844	0.011403
C_0	82.34	3.81209	88.4632	0.012143

The reliability of T_1, T_2, D_1, D_2 and C_0 is obtained by Monte Carlo Weibull distribution fitting, respectively, as shown in Fig. 18 the reliability of T_2 decreases rapidly and the B10 lifetime is only about 19.4 years.

In this article, to analyze one of the characteristics of IGBT degradation with time, and ensure that the degradation process can be directly reflected in the change of failure rate, the thermal network updating method is utilized to assume the fatigue accumulation process of solder layer. According to the relationship between the life and failure rate shown in (25) which obeys the reliability exponential distribution [12], the segmented failure rate calculation containing the damage changes with the service time is shown in Fig. 19. With the increase of service time, the failure rate and damage of each interval are not equal, which is mainly caused by the difference between the gradual aging of devices from the initial state and the direct use of aging devices.

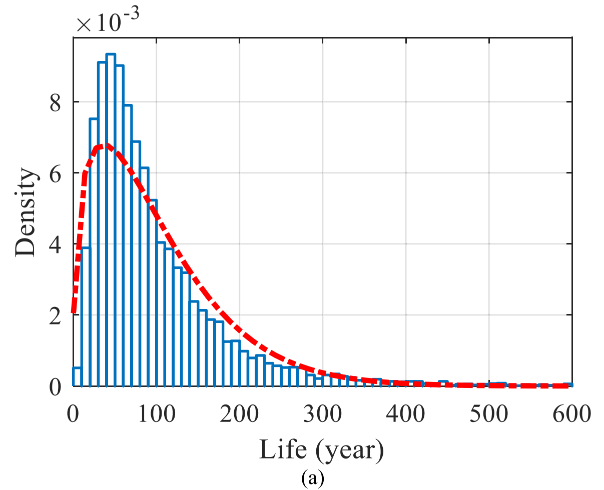

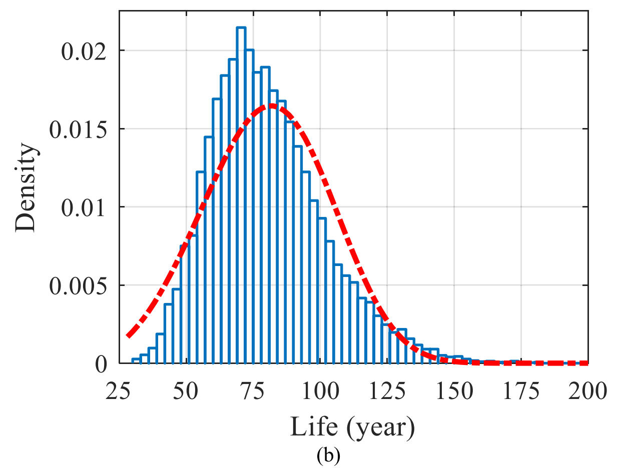

FIGURE 17. Monte Carlo simulation result fitted by Weibull distribution. (a) T_2. (b) C_0.

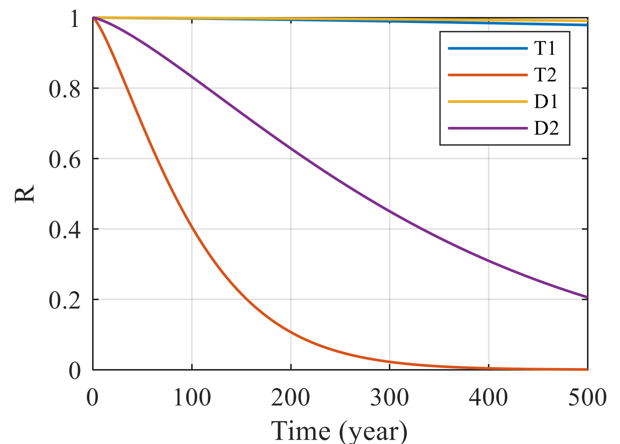

FIGURE 18. Reliability of components by using Weibull distribution.

$$L_i D_i = 1 \tag{24}$$

$$L_i = MTTF = \int_0^\infty e^{-\lambda_i t} = \frac{1}{\lambda_i}, \quad i = 1, \ldots n \tag{25}$$

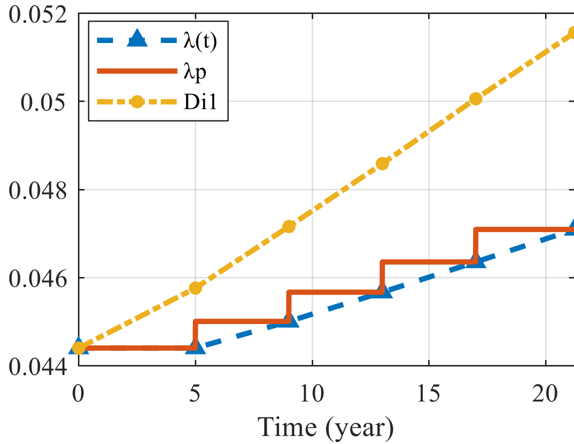

FIGURE 19. The annual damage and failure rate of T2 vary with the increase of service time.

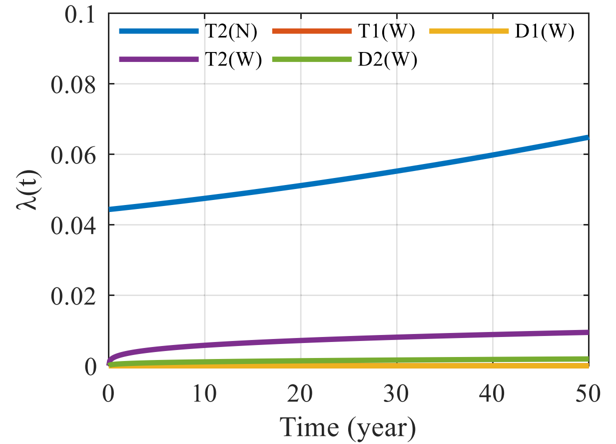

FIGURE 20. Comparison of failure rate under improved method and Weibull distribution.

$$L_i = \sum_{i=0}^{t_i} \frac{L_{i1}}{D_{i1}} \tag{26}$$

$$L_{i1} = t_i - t_{i-1}, \quad t_0 = 0 \tag{27}$$

$$\lambda_i = \frac{1}{\sum_{i=0}^{t_i} (L_{i1} \times \frac{100\%}{D_{i1}})} \tag{28}$$

where D_i represents the total damage in the period of time $(0, t_i)$ while predicted lifetime value is L_i, L_{i1} is the time required in (t_{i-1}, t_i) time when the stage damage is D_{i1}, and λ_i is the failure rate in the current situation. The degradation process of a certain physical characteristic of IGBT with time can be divided into several stages, and the reliability and failure rate of each stage under exponential distribution are calculated in followings

$$R_p(t) = e^{-\lambda_i t} \quad i = 1, \ldots, n \tag{29}$$

$$\lambda_i(t) = \begin{cases} \lambda_1 & 0 < t < t_1 \\ \lambda_2 & t_1 < t < t_2 \\ \vdots & \\ \lambda_n & t_{n-1} < t < t_n \end{cases} \tag{30}$$

As presented before, $R_p(t)$ and $\lambda_i(t)$ are the reliability and failure rate of IGBT calculated various stages, n is the number of stages, and (t_{n-1}, t_n) is the time period when the failure rate is λ_n.

The service time-varying failure rate related to the thermal resistance degradation of IGBT solder layer can be obtained by fitting

$$\lambda_v(\mathrm{t}) = at^2 + bt + c \tag{31}$$

Taking T_2 with the highest annual damage as an example, $a = 4.153 \times 10^{-6}$, $b = 4.162 \times 10^{-5}$, $c = 0.04438$. Comparing the failure rate and device level reliability under Weibull distribution of Fig. 20 and Fig. 21, it is found that the failure rate obtained by this method is higher and more conservative, and the fitting result of a segmented function

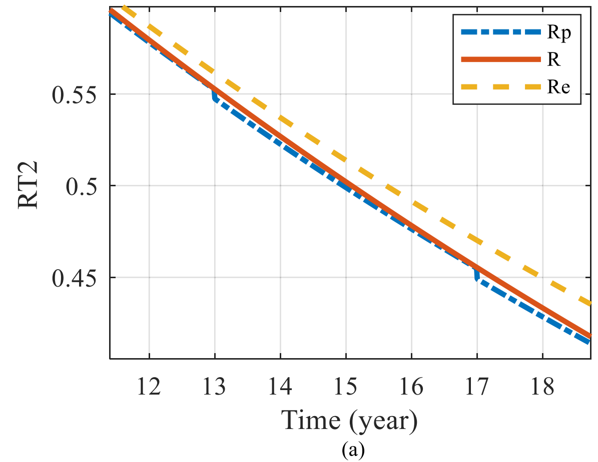

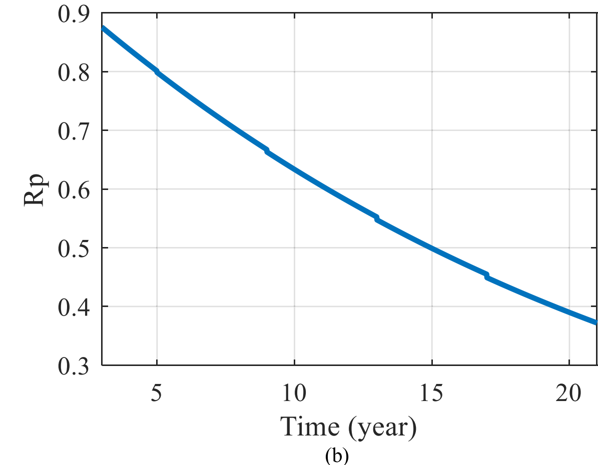

FIGURE 21. T_2 reliability under different analysis (a) and piecewise function (b) with performance degradation.

is better in the service time of T_2. T_2(W) means the failure rate calculated by Weibull distribution while T_2(N) represents the analysis under improved exponential distribution. The huge difference in failure rate comes from the different calculation methods under different reliability distribution

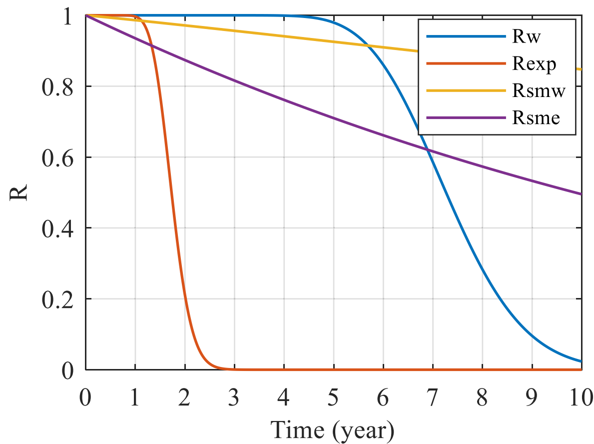

FIGURE 22. MMC submodule and system reliability with different analytical approaches.

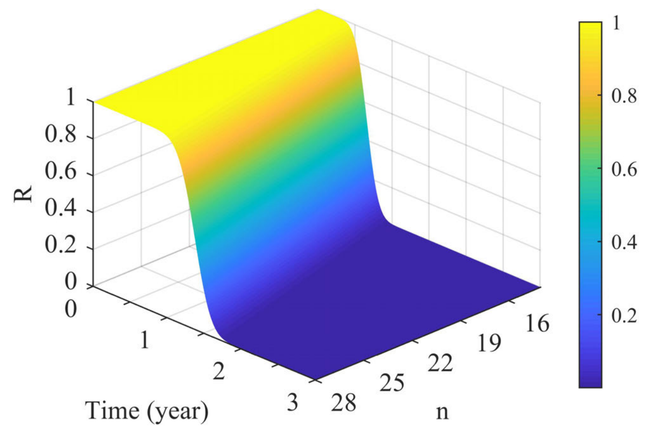

FIGURE 23. System reliability varies with redundancy and time.

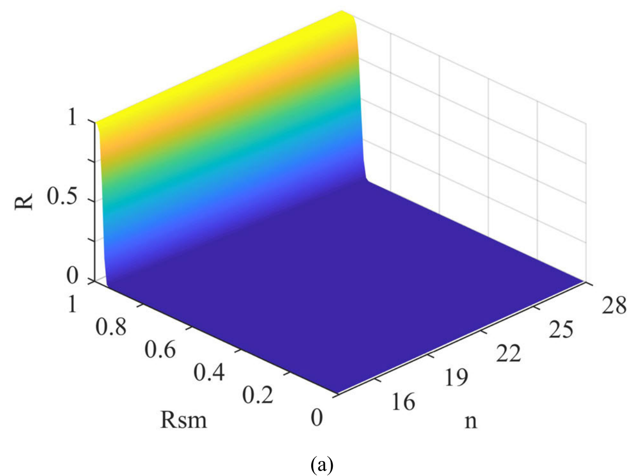

(a)

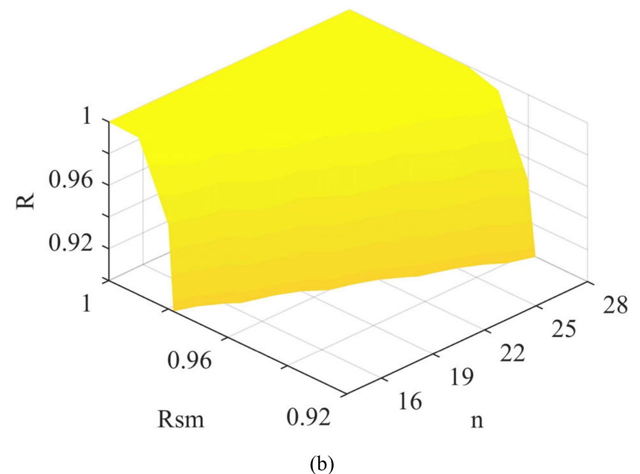

(b)

FIGURE 24. The relationship between system reliability, submodule reliability and redundancy.

functions. In Fig. 21, compared with traditional exponential method R_e, the piecewise exponential distribution R_p and simplified fitting result R are able to describe aging failure rate with working time. Therefore, the method can directly get the increasing failure rate according to the degradation of physical parameters, and improve the reliability exponential distribution model with constant failure rate.

B. REDUNDANCY DESIGN WITH RELIABILITY CONSIDERATION

With the utilization of k/n(G) model [10], we are able to get access to the reliability of MMC system with active redundancy [13]

$$R = \left[\sum_{i=N}^{n+N} \binom{n+N}{i} R_{sm}^{i} (1 - R_{sm})^{N+n-i}\right]^{6} \tag{32}$$

where R_{sm} is the reliability of submodules, n is the number of modules in normal operation of the bridge arm, and N is the number of redundant modules. Substituting R_{smw} under Weibull distribution and R_{sme} under exponential distribution into (32), respectively, the system reliability R_w and $R_{\exp}$ of MMC shown in Fig. 22 can be obtained.

Through the analysis of Fig. 23 and Fig. 24, in order to ensure that the system level R is higher than 0.9, the reliability R_{sm} of submodules should be higher than 0.92. Apply multi-objective function to optimize the number of redundant modules [25], ensure the maximum R and the minimum redundancy. The redundancy rate can be calculated in (33), while (34) is the redundancy optimization function, and R_v of equation (35) is the reliability growth rate.

$$\delta = \frac{n}{N} \tag{33}$$

$$A = \frac{n}{\delta(N+n)} = \frac{N}{N+n} \tag{34}$$

$$R_v = \frac{dR}{dn} \tag{35}$$

Determine the objective function is T, and the weight is w. When we get T at the maximum value, it is the optimal number of redundant submodules at the current weight.

$$T = w_1 R + w_2 A + w_3 R_v \tag{36}$$

$$w_1 + w_2 + w_3 = 1 \tag{37}$$

$$T_{\max} = \max\{w_1 R + w_2 R_v + w_3 A\} \tag{38}$$

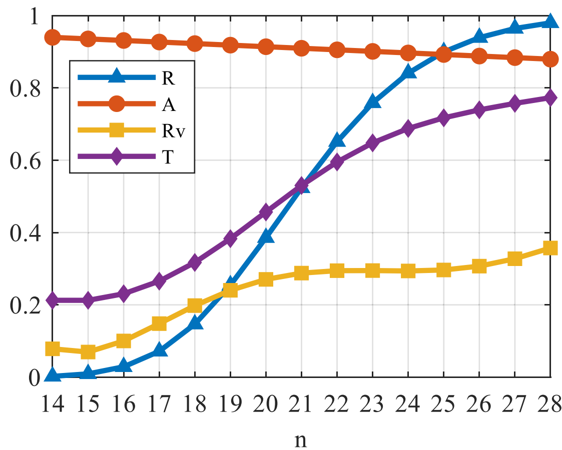

FIGURE 25. Process of multi-objective function optimization.

As an implemental example, Fig. 25 shows the objective function optimization process with n redundant modules under 232 operation submodules, optimized numbers are evaluated at $w_1 = 0.5$, $w_2 = 0.3$, $w_3 = 0.2$, $R_{sm} = 0.935$ which is evaluated after a year profile.

The multi-objective function optimization is based on fundamental 232 modules in each arm, the redundant number of submodules is between 14-28 according to the engineering experience of 8%-12% redundancy. In the efficiency optimization of reliability improvement, the number of modules is balanced between system level reliability R and reliability growth rate R_v.

Considering the economic factor, redundant submodule number optimization function A is directly related to additional cost and reliability R should be as large as possible, so the intersection of the two lines is the reliability optimization result of redundant submodules considering the cost. Therefore, in the higher range of T and R_v, the intersection point n = 25 of A and R is taken as the optimal value to balance the cost and reliability.

According to (39) given in reference [14], [26] and the price of selected IGBT [27], the additional cost (40) can be evaluated when the key components of submodules are considered

$$\Sigma_{film} = a_f + b_f V_r + c_f C_r \tag{39}$$

$$C_{add} = n(2(C_{IGBT} + C_{driver}) + \Sigma_{film}) \tag{40}$$

where $a_f = -1.2\$$, $b_f = 0.06\$/V$, $c_f = 2.7\$/mF$, $C_{IGBT} = 1967\$$ and C_{driver} is around 350$ per unit. As a multi-objective optimization function, T can be used as a reference to judge whether the optimization is effective in this condition.

V. CONCLUSION

From the viewpoint of the operating condition stress analysis and the degradation degree of MMC submodule key device, the paper proposes a failure conversion method considering operating conditions as well as device aging, which improves traditional exponential reliability analysis and optimizes the redundancy design with the objective function.

In terms of the component level failure rate and reliability analysis, the annual temperature mission profile and the power mission profile under MMC operation condition are processed by the rainflow algorithm at first. The thermal network updating is implemented to calculate the lifetime in sections, and the time-varying failure rate for single device degradation can be obtained as an input of the failure rate conversion method. Weibull distribution fitting by Monte Carlo simulation and exponential distribution are analyzed to compare the improved method. The results show that the efficiency of the proposed method is quite different from that of Monte Carlo method when considering the aging of devices, and the failure rate changes more obviously with the aging of single-device than traditional exponential distribution.

While the evaluation of failure rate and reliability has been done, the redundant system level reliability is evaluated with the k/n(G) model. The reliability related system analysis as well as design are performed, which is based on the calculation results of device aging failure rate conversion under operating condition. For redundancy and system level reliability, a multi-objective optimization function is established and the optimal number of redundant modules considering cost trade-off has been carried out.

REFERENCES

[1] A. Lesnicar and R. Marquardt, "An innovative modular multilevel converter topology suitable for a wide power range," in *Proc. IEEE Bologna Power Tech Conf.*, Bologna, Italy, vol. 3, Jun. 2003, p. 6.

[2] Y. Yang, A. Sangwongwanich, and F. Blaabjerg, "Design for reliability of power electronics for grid-connected photovoltaic systems," *CPSS Trans. Power Electron. Appl.*, vol. 1, no. 1, pp. 92–103, Dec. 2016.

[3] L. Wang, J. Xu, G. Wang, and Z. Zhang, "Lifetime estimation of IGBT modules for MMC-HVDC application," *Microelectron. Rel.*, vol. 82, pp. 90–99, Mar. 2018.

[4] H. Liu, K. Ma, Z. Qin, P. C. Loh, and F. Blaabjerg, "Lifetime estimation of MMC for offshore wind power HVDC application," *IEEE J. Emerg. Sel. Topics Power Electron.*, vol. 4, no. 2, pp. 504–511, Jun. 2016.

[5] M. Held, P. Jacob, G. Nicoletti, P. Scacco, and M.-H. Poech, "Fast power cycling test of IGBT modules in traction application," in *Proc. 2nd Int. Conf. Power Electron. Drive Syst.*, Singapore, vol. 1, 1997, pp. 425–430.

[6] I. F. Kovačević, U. Drofenik, and J. W. Kolar, "New physical model for lifetime estimation of power modules," in *Proc. Int. Power Electron. Conf. (ECCE ASIA)*, Sapporo, Japan, Jun. 2010, pp. 2106–2114.

[7] R. Bayerer, T. Herrmann, T. Licht, J. Lutz, and M. Feller, "Model for power cycling lifetime of IGBT modules—Various factors influencing lifetime," in *Proc. 5th Int. Conf. Integr. Power Electron. Syst.*, Nuremberg, Germany, 2008, pp. 1–6.

[8] M. Ciappa, "Selected failure mechanisms of modern power modules," *Microelectron. Rel.*, vol. 42, nos. 4–5, pp. 653–667, Apr. 2002.

[9] Y. Shen, H. Wang, Y. Yang, P. D. Reigosa, and F. Blaabjerg, "Mission profile based sizing of IGBT chip area for PV inverter applications," in *Proc. IEEE 7th Int. Symp. Power Electron. Distrib. Gener. Syst. (PEDG)*, Vancouver, BC, Canada, Jun. 2016, pp. 1–8.

[10] A. Birolini, "Reliability analysis during the design phase (nonrepairable elements up to system failure)," in *Reliability Engineering*. Berlin, Germany: Springer, 2014, pp. 25–80.

[11] S. Bednarz and D. Marriott, "Efficient analysis for FMEA," in *Proc. Ann. Rel. Maintainability Symp.*, 1988, pp. 416–421.

[12] H. S. H. Chung, H. Wang, F. Blaabjerg, and M. Pecht, *Reliability of Power Electronic Converter Systems*. London, U.K.: Institution of Engineering and Technology, 2015, pp. 0885–8993.

[13] J. Guo, X. Wang, J. Liang, H. Pang, and J. Gonçalves, "Reliability modeling and evaluation of MMCs under different redundancy schemes," *IEEE Trans. Power Del.*, vol. 33, no. 5, pp. 2087–2096, Oct. 2018.
[14] P. Tu, S. Yang, and P. Wang, "Reliability- and cost-based redundancy design for modular multilevel converter," *IEEE Trans. Ind. Electron.*, vol. 66, no. 3, pp. 2333–2342, Mar. 2019.
[15] U.-M. Choi, F. Blaabjerg, and K.-B. Lee, "Study and handling methods of power IGBT module failures in power electronic converter systems," *IEEE Trans. Power Electron.*, vol. 30, no. 5, pp. 2517–2533, May 2015.
[16] B. Wang, J. Wang, D. Ma, L. Wang, F. Yang, X. Li, and Y. Tan, "A lifetime estimation method of MMC submodules based on the combination of FEA and physical lifetime model," in *Proc. 10th Int. Conf. Power Electron. ECCE Asia (ICPE-ECCE Asia)*, Busan, South Korea, 2019, pp. 1–6.
[17] *Datasheet of AVX Film Capacitors*. Accessed: Dec. 10, 2019. [Online]. Available: http://www.avx.com/products/film-capacitors/power-film-caps/
[18] P. Li, W. Wang, C. Liu, Y. Huang, Y. Wang, and L. Zhang, "Economic assessment of Zhangbei VSC-based DC grid planning scheme with integration of renewable energy and pumped-hydro storage power station," *Proc. CSEE*, vol. 38, no. 24, pp. 7206–7214, 2018.
[19] *Tsinghua Weather Station Ambient Temperature Data of Beijing, China*. Accessed: Dec. 5, 2019. [Online]. Available: https://climate.dest.com.cn/
[20] M. A. Miner, "Cumulative damage in fatigue," *J. Appl. Mech.*, vol. 12, no. 3, pp. A159–A164, 1945.
[21] W. Lai, M. Chen, L. Ran, O. Alatise, S. Xu, and P. Mawby, "Low ΔTj stress cycle effect in IGBT power module die-attach lifetime modeling," *IEEE Trans. Power Electron.*, vol. 31, no. 9, pp. 6575–6585, Sep. 2016.
[22] B. Gao, F. Yang, M. Chen, Y. Chen, W. Lai, and C. Liu, "Thermal lifetime estimation method of IGBT module considering solder fatigue damage feedback loop," *Microelectron. Rel.*, vol. 82, pp. 51–61, Mar. 2018.
[23] M. Chen, Y. Chen, B. Gao, W. Lai, T. Huang, and S. Xu, "Lifetime evaluation of IGBT module considering fatigue accumulation of solder layers," *Proc. CSEE*, vol. 38, no. 20, pp. 6053–6061, 2018.
[24] M. Makdessi, A. Sari, P. Venet, P. Bevilacqua, and C. Joubert, "Accelerated ageing of metallized film capacitors under high ripple currents combined with a DC voltage," *IEEE Trans. Power Electron.*, vol. 30, no. 5, pp. 2435–2444, May 2015.
[25] B. Wang, F. Tan, and J. Shang, "Optimal configuration of modular redundancy for MMC," *Electr. Power Automat. Equip.*, vol. 35, no. 1, pp. 13–19, 2015.
[26] R. Burkart and J. W. Kolar, "Component cost models for multi-objective optimizations of switched-mode power converters," in *Proc. IEEE Energy Convers. Congr. Expo.*, Denver, CO, USA, Sep. 2013, pp. 2139–2146.
[27] *Price of Infineon FZ1500R33HL3*. Accessed: Jul. 20, 2020. [Online]. Available: https://www.mouser.com/ProductDetail/Infineon-Technologies/FZ1500R33HL3?qs=%2Fha2pyFadujpWdAGE0TDaLAiA8Gov%2FwpdiHfe0RbkQLrOD3a0Y%2FqJw==&utm_source=octopart&utm_medium=aggregator&utm_campaign=641-FZ1500R33HL3&utm_content=Infineon
[28] B. Li, R. Yang, D. Xu, G. Wang, W. Wang, and D. Xu, "Analysis of the phase-shifted carrier modulation for modular multilevel converters," *IEEE Trans. Power Electron.*, vol. 30, no. 1, pp. 297–310, Jan. 2015.
[29] P. M. Meshram and V. B. Borghate, "A simplified nearest level control (NLC) voltage balancing method for modular multilevel converter (MMC)," *IEEE Trans. Power Electron.*, vol. 30, no. 1, pp. 450–462, Jan. 2015.

GAOTAI LV (Graduate Student Member, IEEE) received the B.S. degree in physics from Lanzhou University, Lanzhou, China, in 2017. He is currently pursuing the M.S. degree in electrical engineering with Xi'an Jiaotong University, Xi'an, China. His research interests include modular multilevel converters and reliability of power electronic systems.

WANJUN LEI (Member, IEEE) received the B.S., M.S., and Ph.D. degrees in electrical engineering from Xi'an Jiaotong University, Xi'an, China, in 2000, 2004, and 2008, respectively.

He is currently an Associate Professor with the School of Electrical Engineering, Xi'an Jiaotong University. His research interests include active power filters, power electronics inverters, reactive power compensation, and power quality control techniques.

Dr. Lei is a member of the China Power Supply Society.

MENG WANG was born in Shandong, China, in 1995. He received the B.S. degree in electrical engineering from Northeast Dianli University, Jilin City, China, in 2018. He is currently pursuing the M.S. degree with the School of Electrical Engineering, Xi'an Jiaotong University, Shaanxi, China. His research interests include reliability of high-power power electronic devices and on-line monitoring of capacitors.

CHUNLIN LV (Graduate Student Member, IEEE) received the B.S. degree in electrical engineering from Chongqing University, Chongqing, China, in 2018. He is currently pursuing the Ph.D. degree in electrical engineering with Xi'an Jiaotong University, Xi'an, China. His research interests include reliability modeling of capacitors, reliability evaluation of power electronic systems, and optimization design of power electronic systems.

JIAQI ZHAO received the B.S. degree in electrical engineering from Nanjing Normal University, Nanjing, China, in 2019. She is currently pursuing the M.S. degree in electrical engineering with Xi'an Jiaotong University, Xi'an, China. Her research interest includes large capacity power electronic equipment reliability quantitative evaluation and design.